UC Irvine
UC Irvine Previously Published Works

Title

Genomic profiling of Sézary syndrome identifies alterations of key T cell signaling and differentiation genes

Permalink

https://escholarship.org/uc/item/58813453

Journal

Nature Genetics, 47(12)

ISSN

1061-4036

Authors

Wang, Linghua
Ni, Xiao
Covington, Kyle R
et al.

Publication Date

2015-12-01

DOI

10.1038/ng.3444

Peer reviewed

Genomic profiling of Sézary Syndrome identifies alterations of key T-cell signaling and differentiation genes

Linghua Wang[1], **Xiao Ni**[2], **Kyle R. Covington**[1], **Betty Y. Yang**[2], **Jessica Shiu**[2], **Xiang Zhang**[2], **Liu Xi**[1], **Qingchang Meng**[1], **Timothy Langridge**[2], **Jennifer Drummond**[1], **Lawrence A. Donehower**[3], **Harshavardhan Doddapaneni**[1], **Donna M. Muzny**[1], **Richard A. Gibbs**[1], **David A. Wheeler**[1], and **Madeleine Duvic**[2]

[1]Human Genome Sequencing Center, Baylor College of Medicine, Houston, TX 77030, USA.

[2]Department of Dermatology, the University of Texas MD Anderson Cancer Center, Houston, Texas 77030, USA.

[3]Department of Molecular Virology and Microbiology, Baylor College of Medicine, Houston, Texas 77030, USA.

Abstract

Sézary Syndrome is a rare leukemic form of cutaneous T-cell lymphoma defined as erythroderma, adenopathy, and circulating atypical T-lymphocytes. It is rarely curable with poor prognosis. Here we present a multi-platform genomic analysis of 37 Sézary Syndrome patients that implicates dysregulation of the cell cycle checkpoint and T-cell signaling. Frequent somatic alterations were identified in *TP53, CARD11, CCR4, PLCG1, CDKN2A, ARID1A, RPS6KA1,* and *ZEB1*. Activating *CCR4* and *CARD11* mutations were detected in nearly a third of patients. *ZEB1*, a transcription repressor essential for T-cell differentiation, was deleted in over half of patients. *IL32* and *IL2RG* were over-expressed in nearly all cases. Analysis of T-cell receptor Vβ and Vα expression revealed ongoing rearrangement of the receptors after the expansion of a malignant

clone in one third of subjects. Our results demonstrate profound disruption of key signaling pathways in Sézary Syndrome and suggest potential targets for novel therapies.

Cutaneous T-cell lymphomas (CTCL), are heterogeneous lymphoproliferative disorders of clonal skin homing T-cells. Sézary Syndrome (SS), the leukemic variant of Mycosis Fungoides (MF), is defined as erythroderma (80% redness of the skin, adenopathy and   1,000/μL circulating Sézary cells with a CD4+CD26− or a CD4+CD7− phenotype[1-4]. SS cells have a type 2 helper T cell (Th2) cytokine profile[1-4]. Other features are Staphylococcus aureus colonization, eosinophilia, high IgE levels, chronic, keratoderma with tinea, leonine facies, and secondary malignancies[5,6]. Depletion of the T-cell repertoire diversity or complexity may cause profound immunosuppression and susceptibility to lethal infection with Cytomegalovirus and *S. aureus*[7,8]. SS has a median overall survival of only 2.4 years in patients with >10,000/μL Sézary cells or 5.4 years in patients with 1000–10,000/μL Sézary cells[9-12].

MF and SS are the most common CTCLs. SS can arise *de novo* or it can appear following years of chronic MF[1,12], suggesting these two diseases are related at some deeper level. MF and SS are thought to arise from clonal expansion of CD4+ helper T-cells responding to chronic antigen stimulation. Loss of Fas/Fas ligand mediated activation-induced cell death causes accumulation of the clones which may acquire mutations[13,14].

Until now, molecular genetic features of SS were limited to small patient cohorts, derived from a single molecular platform. Early cytogenetics and array comparative genomic hybridization (aCGH) approaches[15-19] revealed focal deletions of *TNFAIP3*[20], *CDKN2A*[21]. Mutation of *TP53*[22] reported in a small study, precluded assessment of population frequencies. Recently, targeted sequencing of CTCL patients revealed novel mutations in *PLCG1* in about 27% of MF patients and 9% of SS patients[23]. Genomic gains and point mutations of *TNFRSF1B,* encoding TNFR2, were recently reported in 18% of MF and SS patients[24]. Seventeen genes with mutations and loss of tumor suppressors were very recently reported using genomic sequencing with RNA-seq[25]. PLCG1 and TNFR2 are critical mediators of T-cell receptor (TCR) signaling. Genomic sequencing is shedding new light on the mechanisms of CTCLs and offer new options for targeted therapy.

Although there are several therapies under evaluation that target T-cells, none have led to a cure[6,26,27]. Hence, our efforts focused on comprehensive, cross-platform integrated analysis of patients with Sézary Syndrome, with attention towards dissecting the molecular pathogenesis and identifying novel clinically actionable molecular targets.

RESULTS

Clinical and histopathological data

A total of 37 SS patients with significant blood involvement (Stage IVA or IVB) were enrolled in the discovery study. All patients provided informed consent for genomic analysis and Institutional Review Boards approved tissue collection. Eleven patients had a preceding history of MF. The clinical and histopathological data were summarized in **Supplementary Table 1**. CD4+ T-cells were isolated from the peripheral blood of SS patients (**Online**

Methods). We confirmed the identity of Sézary cells as CD4^{+}CD26^{−} cells with a Th-2 phenotype by examining the expression of cell surface markers and Th1/Th2 cytokine expression profiles of the patients (**Supplementary Fig. 1**). A skin biopsy from each patient's sun-shielded skin was used to culture and expand fibroblasts, from which genomic DNA was extracted and used as matched control for whole-exome sequencing (WES) and SNP array analyses. In addition, CD4^{+} T-cells were isolated from five healthy donors and their mRNAs were used as controls for whole transcriptome sequencing (RNA-seq). An extension cohort of 68 patients was included and genomic DNAs were extracted from their peripheral blood mononuclear cells (PBMCs). The experimental details were summarized in **Supplementary Table 2**.

Somatic mutations

WES was performed on tumor and matched fibroblast DNAs as described previously[28], yielding a mean coverage of 100×, approximately 94% of targeted bases were covered to a depth of 20× or more. A total of 4,738 somatic mutations were identified (**Supplementary Table 3**). Validation of mutations in 35 recurrently altered genes was accomplished using a custom capture array (NimbleGen, Inc., **Supplementary Table 4**) and deep sequencing. The validation rates were 100% for substitutions and 93% for small insertions and deletions (**Supplementary Table 5**). In addition, for the 32 patients with RNA-seq data available, the mutant alleles of 1,090 somatic mutations were expressed in their mRNAs (**Supplementary Table 3** and **Supplementary Fig. 2**).

The average somatic mutation rate was 3.85 mutations per megabase (Mb) of targeted DNA and the non-synonymous mutation rate was 2.75 mutations per Mb (**Supplementary Fig. 3**), which is comparable to adult solid tumors[29,30]. The most frequent substitution was the cytosine to thymine (C>T) transition (**Fig. 1**) averaging 74% of mutations across the cohort. As shown in **Supplementary Fig. 4a**, this high C>T frequency was attributable to two separate mutational processes: 43% of the C>T were at NpCpG sites, which is regarded as age-related[31] resulting from spontaneous deamination at CpG sites; 30% of the C>T were at NpCpC sites, T being most prevalent 5' nucleotide for the signature of UVB exposure[31]. The fraction of UVB signature in SS is much higher than that of other liquid tumor types (ALL and AML) but is similar to that of cutaneous squamous cell carcinoma (CSCC), see **Fig. 1b**. Consistent with the prevalence of UVB mutagenesis, a relatively large fraction (2.2%) of dinucleotide mutations (DNM) were found; 68.3% of those were CC>TT. The UVB is a powerful mutagen, which increases the overall mutation frequency. Consistent with this, the signature fractions correlated significantly with overall mutation frequencies (**Supplementary Fig. 4b**). Prior MF phase has no effect on the amount or percentage of UVB signature observed in a subject ($P = 0.15$). Although 13 patients received prior focal skin UVB or UVA treatment, no correlation was observed between the presence of UVB signature and the history of therapeutic UV exposure (**Supplementary Fig. 4c**). This indicates that the accumulated life-time exposure to UV radiation alone explains these UV signatures of SS patients, and is challenging the view that SS originates from the memory T-cells that were in circulation (central memory, Tcm), rather than those resident in the skin (resident memory, Trm)[32].

Two genes, *TP53* and *CCR4* were determined to be cancer drivers based on mutation frequency evidence alone in the discovery cohort (**Supplementary Table 6**). We identified three additional likely driver genes by augmenting mutation frequency with evidence from expression data, functional impact, and known cancer-related genes: *ARID1A*, *CARD11*, *FAS* (**Supplementary Table 7**). To verify the mutation prevalence of these genes, targeted deep sequencing (1200× fold coverage) of 35 selected genes (**Supplementary Table 4)** was performed in an extended cohort of 68 SS patients. For genes with hotspot mutations and genes with frequent inactivating mutations, we are able to replicate mutation frequencies in the extension set (**Fig. 2a**, **Supplementary Fig. 5**, and **Supplementary Table 8**). We identified proportionately more *PLCG1* mutations in the extension cohort (**Supplementary Table 9)**. The most frequently mutated genes in the combined cohorts were: *TP53* (24%), *PLCG1* (18%), *CARD11* (15%), *ARID1A* (10%), *FAS* (10%), *CCR4* (7%), *RHOA* (7%), and *TNFRSF1B* (6%).

TP53 was the most frequently mutated gene (**Fig. 2a**). In ten out of eleven patients in the discovery cohort, the somatic mutations were accompanied by copy number losses (del *17p*). In the discovery cohort, over half (6/11) of *TP53* mutations were located at the canonical splice sites. The mutant alleles of all *TP53* splicing mutations were expressed and changes of *TP53* exon usage accompanied 4 out of 5 splice-site mutations (data not shown).

The chemokine receptor encoded by *CCR4* is important for T-cell migration into skin[33,34]. Overexpression of *CCR4* was reported in SS[35] and as a result anti-*CCR4* therapy is underway with promising early results in MF/SS patients[35,36]. Recently, gain-of-function, C-terminal *CCR4* mutations were reported in 26% of adult T-cell leukemia/lymphoma (ATLL), a disease caused by human T-cell lymphotropic virus-I[37], which like SS also exhibits "skin-homing" pathophysiology. In our SS cohort, 7% of patients harbored *CCR4* somatic mutations and all of them were located at the C-terminus including the recurrent Y331X, Q330X, and 3 novel sites that were not previously reported (**Fig. 2a**). All *CCR4* mutations were either nonsense or frameshift. Moreover, the *CCR4* mutations were heterozygous and tended to be transcribed at lower levels than patients with wild-type *CCR4* (**Fig. 2b,** *P* > 0.05 with n = 5 patients), consistent with a functional role as activating mutations.

CARD11, mutated in 15% of SS patients (**Figs. 1** and **2a**), is a multi-domain adaptor protein required for T cell receptor (TCR)-mediated activation of NF-κB signaling, and is a critical regulator of both T and B cell activation and function[38-40]. Activating *CARD11* mutations were reported in 9.6% of diffuse large B cell lymphoma (DLBCL), virtually all affecting the two coiled-coil domains[41,42] located at N-terminal of the protein (**Fig. 2a**). Introduction of *CARD11* mutants of both coiled-coil domains resulted in constitutive NF-κB activation in lines of both T and B origin[42]. In our combined cohort, we identified 16 *CARD11* mutations, half of which were located within the second coiled-coil domain. The remaining was at a new hotspot located off the N-terminal side of the PDZ domain (**Fig. 2a**). All the mutated positions in this new hotspot are at highly conserved residues (**Supplementary Fig. 6**). Additionally, a *CARD11-PIK3R3* fusion (**Supplementary Table 10**) was detected in a *CARD11*-wildtype patient, which includes the new hotspot region but not the N-terminal coiled-coil domains. *CARD11* expression was significantly increased in patients with both wildtype and mutant *CARD11,* including the fusion transcript, in comparison to that of

healthy donors (**Figure 2b**). These data provide strong evidence of a role for *CARD11* in SS and therefore therapies targeting *CARD11* signaling could benefit SS patients as was previously suggested for *CARD11*-mutated DLBCL[42].

PLCG1, a key mediator in TCR signaling is recently found to be mutated in 27% of MF patients and 9% of SS patients[23]. Five *PLCG1* mutations were identified in the discovery cohort (**Fig. 2a**), but none were at reported sites. In the extension cohort, the frequency of *PLCG1* mutations increased to 21% (14/68), from 14% (5/37) in the original, though not significantly different ($P > 0.05$, **Supplementary Table 9**). In addition to the reported hotspot mutation S345F, we identified a new hotspot R48W in the C-terminal of the protein (**Fig. 2a** and **Supplementary Fig. 7**). Further correlation analysis with SS origin showed that *PLCG1* R48W mutation frequency is significantly higher ($P = 0.041$) in patients evolved from MF (15%) than those occurred *de novo* (3%).

Other somatically mutated genes determined to be likely drivers were *ARID1A*, *FAS*, *TNFRSF1B*, and *RHOA*. As shown in **Supplementary Fig. 5** and **Supplementary Table 9**, recurrent mutation of these genes was replicated in the extension cohort. Most of *ARID1A* mutations were inactivating, consistent with the usual pattern of *ARID1A* mutations observed in other cancers. Likewise, most of *FAS* mutations were inactivating. Given the reported down-regulation of *FAS*, a pro-apoptotic death receptor[43,44], inactivating *FAS* mutations in 7 patients reinforced their putative role in aiding survival of these malignant cells. *TNFRSF1B* Thr377Ile mutation was recently reported in 5% of MF/SS patients[24]. Expression of this mutation in T cells leads to enhance non-canonical NF-κB signaling[24]. We identified six mutations in this gene; one of them was Thr377Ile and the other five mutations were clustered together, indicating a potential mutation hotspot (**Supplementary Fig. 5**). Finally, seven missense mutations with likely functional impact were observed in *RHOA*, a small GTPase that acts to regulate actin cytoskeleton and cell division.

Somatic copy number alterations

Somatic DNA copy number analysis revealed frequent genomic gains and losses (**Fig. 2c**). We identified *CDKN2A* focal deletion in 58% of the patients, compared to about 40% previously reported[21,25]. *CDKN2A* expression was significantly decreased in patients with homozygous deletions (**Fig. 2d**), as expected.

The most frequent novel event in our discovery cohort was a 0.6-Mb focal deletion at *10p11.23* including *ZEB1* and *ZNF438* observed in 56% of the patients (**Fig. 2c**). Of the two genes, only *ZEB1* expression was decreased in proportion to copy number (**Figure 2d**), compared to patients with diploid *ZEB1* (P < 0.001), suggesting that *ZEB1* may be the target of selection within this focal deletion. *ZEB1,* also known as T-cell transcription factor 8, is a zinc finger transcriptional repressor that harbors two independent repressor domains; the N-terminal one blocks the activity of hematopoietic transcription factors such as *ets* and *c-myb* and regulates hematopoietic differentiation[45]. *ZEB1* has been suggested to be critical for early T-cell development[46] and has a role in enhancing transforming growth factor-β1 (TGF-β1) signaling by binding phosphorylated Smad3 and Smad7[47]. *ZEB1* downregulation

contributes to resistance to TGF-β1-mediated growth suppression in ATLL-derived cell lines[47,48]. Loss of *ZEB1* may play a similar role in SS pathogenesis.

Hemizygous deletion of *1p36.1* (33%) encompassed 6 genes including *ARID1A* and *RPS6KA1*. Expression levels of both *ARID1A* and *RPS6KA1* decreased and correlated significantly with their copy number status (**Figure 2d**), suggesting selection operating on these two genes. As mentioned above, six patients in our combined cohorts harbored inactivating mutations in *ARID1A* (**Supplementary Fig. 5**), consistent with the function of *ARID1A* as an epigenetic tumor suppressor. Although *ARID1A* is best known as a component of the SWI/SNF chromatin remodeling complex, recent functional studies suggested a role of *ARID1A* in cell cycle checkpoint machinery, possibly through p53- and/or pRb-dependent signaling cascades[49]. *ARID1A* is required for cell cycle exit, since in the absence of functional *ARID1A*, cell cycle arrest is delayed[50]. *RPS6KA1* is a serine/ threonine kinase that plays a pivotal role in growth factor induced G2/M transition delay and is required to maintain genomic integrity during growth factor stimulation[51] Thus we place these two genes in an ensemble of mutated genes, the dysregulated replication cycle in Sézary cells (**Fig. 3a**).

Finally, focal deletion of *2q37.3* involving *PDCD1* and 5 other genes in 36% of patients (**Figure 2c**). Subjects with *2q37.3* deletion tend to have a worse prognosis ($P = 0.05$), see **Supplementary Fig. 8**. *PDCD1* is expressed on activated T cells and transduces a negative signal that suppresses T-cell function[52]. *PDCD1* is suggested to be a promising immunotherapeutic target in cancer since blockage of *PDCD1* and its ligands can enhance functioning of cytotoxic T cells[53]. However, we observed weak correlation between expression and copy number for *PDCD1,* or any of the 5 known genes in the region (**Supplementary Fig. 9**).

Fusion transcripts and differentially expressed genes

We identified 41 in-frame fusion transcripts by RNA-seq (**Supplementary Table 10**). For 29 fusion transcripts with RNAs available, we performed RT-PCR (**Supplementary Table 11**), sequenced the RT-PCR products and successfully validated all of them. In addition to the aforementioned *CARD11-PIK3R3*, *CD28-CTLA4/ICOS*, and *IKZF2-GLI2* fusions were observed. *CD28* is essential for T-cell proliferation and survival. Low frequency of *CD28-CTLA4* fusion was recently reported in CTCL[24]. *IKZF2* regulates lymphocyte development. Overall, gene-gene fusions appeared to be relatively rare in SS pathogenesis.

To identify differentially expressed genes, we performed an unbiased analysis of the expression data for all detectable transcripts (> 40,000). A total of 345 transcripts were significantly upregulated in SS patients (**Supplementary Table 12**). Gene set enrichment analysis of these genes suggested significant enrichment of only a few canonical pathways (**Supplementary Table 13**), among which were cell cycle control, regulation of immune system, MYC transcriptional activation, and chemokine signaling.

Among those 345 genes, several interleukins (ILs), interleukin receptors, CD molecules, and chemokines that are required for T-cell development and function were strongly upregulated including *IL32, IL2RG, CD3G, CD27, CCR4,* and *CCR8* (**Figure 4a**). *IL2RG*, encoding the

IL2 receptor common gamma chain, was highly expressed in all patients. IL2RG heterodimerizes with several other receptors and may transmit enhanced cytokine signaling to Sézary cells. *IL32* was the most upregulated chemokine (**Figure 4b**); and strongly upregulated in all but one patient, who had a low level of Sézary cells. Interestingly, *IL32* expression levels were positively correlated with those of *IL2RG* and *CARD11* (**Supplementary Fig. 10a,b**). *IL32* is a pro-inflammatory cytokine expressed by activated T cells and natural killer cells with an important role in T-cell communication, tumorigenesis and autoimmune disease[54]. *IL32* accelerates the proliferation of CTCL cell lines through mitogen-activated protein kinase and NF-κB-mediated signaling[54]. A high level of *IL32* expression in skin lesions of MF patients was reported to correlate with disease activity[54,55].

We examined IL32 protein in CTCL cell lines and tumor cells from a subset of SS patients. IL32α was not detectable in the serum of SS patients or the cell culture supernate of any cell lines (data not shown), suggesting that IL32α might function intracellularly rather than intercellularly in the context of SS cells. Western blot employing a purified anti-human IL32 monoclonal antibody, which has been shown to bind to all isoforms of IL32[56], showed a strong single 24-kDa± band, indicative of IL32 β translation in all cell lines (**Fig. 4c**). IL32 protein expression in patients' cells was more heterogeneous exhibiting both the α and β isoforms in some patients (**Fig. 4d**). Overall, the protein expression is correlated with their mRNA expression and the density of Sézary cells in their blood. These data support the possibility that IL32 is involved in an autocrine signaling loop stimulating growth of Sézary cells as suggested by Suga and colleagues[54].

Dysregulated signaling pathways

Our integrated genomic analyses revealed frequent alterations primarily in three oncogenic pathways (**Supplementary Table 14**): epigenetic regulation (95%), TCR signaling (84%) and cell cycle control (78%). Importantly, we identified frequent alterations in genes involved in cell cycle control, especially genes that regulate G1/S and G2/M checkpoints (**Fig. 3a**). Notably, multiple genes were recurrently altered at a high frequency, including the aforementioned *TP53, CDKN2A, ARID1A* and *RPS6KA1*, suggesting that loss of mitotic checkpoint control might be an important contributor to the high rate of genomic instability observed in SS patients.

Additionally, we identified somatic alterations in TCR signaling in 84% of cases (**Fig. 3b**). TCR signaling in response to antigen recognition has a critical role in the adaptive immune response. Recurrent alterations were identified in *CARD11, PLCG1, LAT, RAC2, PRKCQ, CD28,* and genes that encode the calcium channel subunits. Finally, though the epigenetic regulation was most frequently altered, the majority of involved genes were mutated only once each. As shown in **Supplementary Tables 15-16**, all eight classes of epigenetic genes[57] were somatically altered across the cohort with the highest frequency (66%) among the histone writers.

Evolution of the SS TCR repertoire

The orderly rearrangement and assembly of TCR genes during T-cell development creates a polyclonal TCR repertoire that is highly diverse in healthy individuals. An important

diagnostic correlate in CTCL is the identification of a unique TCR rearrangement pattern present in the circulating malignant T-cells, indicative of an expanded T-cell clone[58]. With RNA-seq data, we were able to assess all V chains simultaneously. All patients' TCR expressed Vα and Vβ and two of them also expressed Vγ and Vδ. We detected one or two dominant Vβ- or Vα-expressing clone(s) in 97% of patients (**Supplementary Table 17**), compared to 67% by flow cytometric analysis of TCR-Vβ using fluorescence-labeled monoclonal antibodies.

Our analysis revealed varied patterns in the dominant Vβ and Vα receptors (**Fig. 5a,c**). We detected mono-, bi-, and polyclonal TCR-Vβ in 56%, 22%, and 22% of patients respectively, and mono-, bi-, polyclonal TCR-Vα in 66%, 22%, and 12% of patients, respectively (**Supplementary Table 17**). The most frequent clonally expanded TCR-Vα gene was *TRAV27*, followed by *TRAV9-2*. The most frequent clonally expanded TCR-Vβ gene was *TRBV20-1,* followed by *TRBV7-3* (**Supplementary Fig. 11**). *TRBV20-1* is associated with *S. aureus* infection[59], a common feature of SS, and a finding consistent with the antigen-stimulation theory of CTCL[60].

The TCR is thought to be formed by differentiation of a T-cell precursor in the thymus[61,62] in which, critically, the Vβ locus is rearranged and expressed on the cell surface, followed by rearrangement of the Vα locus. The T-cells with fully formed, heterodimerized TCR exit the thymus and live in various body compartments until stimulated by antigen. Upon malignant transformation, this simple model of TCR differentiation should lead to a clonal population expressing a single Vα and a single Vβ. In our cohort, 11 out of 32 patients fit the model of a single Vα and Vβ transcript expressed. Interestingly, 6 patients exhibited monoclonal Vβ paired with either a biclonal or poly-clonal Va (**Fig. 5b**). Clearly, at the point of malignant transformation, these cells were able to further differentiate their Vα chain to produce a second Vα receptor (bi-clonal) or even a fully polyclonal Vα repertoire, each of which is paired to a single (clonal) Vβ. This final differentiation step occurs after the malignant transformation event because the malignant cells are clonal with respect to their mutation profile.

Moreover, an additional 7 patients with monoclonal Vα were biclonal or polyclonal in Vβ. Since the canonical differentiation of the TCR stipulates the Vβ rearrangement occurs before the Va[61,62], it is hard to explain how a malignant clone can be monoclonal for Vα and polyclonal for Vβ. One possibility is that some T-cells rearrange the Vα receptor first, contrary to the accepted TCR differentiation pathway; or, alternatively, upon malignant transformation, the initially rearranged Vβ is lost, and a new round of Vβ rearrangement occurs as the malignant cells divide to produce polyclonal Vβ. This latter mechanism would be the simplest one to explain the poly clonality in both the Vα and Vβ. Together, these data suggest greater phenotypic complexity in the display of TCR components than had been previously appreciated.

Correlation and survival analysis

Finally, our correlation and survival analyses confirmed that large cell transformation (LCT) and African ancestry were associated with worse prognosis[11,63] (**Fig. 6a**), which is also replicated in the extension cohort (**Supplementary Fig. 12**). *TP53* mutation and *2q37.3*

focal deletion were significantly enriched in patients with LCT (**Fig. 6b**). Interestingly, we found that prevalence of UVB signature was significantly lower in African American patients while *IL32* expression was significantly higher (**Figure 6c**). Overexpression of *IL32* in African American patients with worse prognosis further suggesting a connection between *IL32* and the pathophysiology of SS. Our survival analysis also suggested a trend towards worse prognosis in patients with *CCR4* alteration, *CDKN2A, 2q37.3* deletion (**Supplementary Fig. 9**).

DISCUSSION

To gain more insight into the genomic basis of SS, we assessed the somatic mutation, DNA copy number and gene expression profiles in 37 patients. In addition to somatic alterations in previously known SS-associated genes such *TP53* and *CDKN2A*, novel recurrent mutations and/or focal deletions were identified in *CARD11, CCR4, PLCG1, ARID1A*, and *ZEB1*, etc. Several somatic alterations are reported to specifically impact T-cell signaling and differentiation. These data coupled with overexpression of *IL32* and *IL2RG,* lend the first mechanistic insights into the nature of SS pathogenesis, and suggest avenues for development of targeted therapies. Importantly, this study has drawn a number of parallels, through shared molecular features, to other malignancies of both B- and T-cell origin. The *CCR4* activating mutations, first reported in ATLL patients, are in common with our SS patients' mutations and highlight the importance of *CCR4* in pathogenesis and targeted therapy of both lymphomas. The mutation of the coiled-coil domain of *CARD11* that potentiates NF-κB signaling in B cells has been recognized as a potential therapeutic target in DLBCL. To these markers, SS adds *IL32* as possible constituents of an autocrine signaling network, which could become targets specific to SS.

Important to the etiology of the disease is a description of the cell of origin of this malignancy and both Tcm and Trm cells have been proposed[32]. The surprising finding of a UVB signature in 30% of the patients is strong evidence that the malignant clonal population arose from a cell that spent a significant time in the superficial layers of the skin, consistent with a Trm origin.

Our data provide evidence of disruption of the precise choreography of TCR maturation, which classically proceeds from Vβ to Vα through multiple rounds of cell division. Production of the same Vα rearrangement in many different Vβ-rearranged cells is difficult to explain by the classical Vβ -> Vα pathway. A mechanism is needed to explain how a cell which presumably exited the thymus with intact TCR-Vα and Vβ heterodimer, restarted the rearrangement of either Vα or Vβ to produce a polyclonal TCR. Thus, the genomic profiling presented here not only added to our understanding of genetic driver mutations, T-cell signaling, but also to the pathophysiology of SS and identified novel targets and pathways for developing more effective therapies.

ONLINE METHODS

Patients

Thirty-seven SS patients from the University of Texas MD Anderson Cancer Center who signed consent were approved by the institutional review board to enroll in this study. It was conducted according to the Declaration of Helsinki Principles. The revised diagnostic criteria for staging of SS by ISCL/EORTC were used[4].

Isolation of CD4+ cells

Peripheral blood was collected prior to therapy from all SS patients using BD Vacutainer® Cell Preparation Tube. Peripheral blood mononuclear cells (PBMCs) were then isolated from granulocytes. CD4+ T-cells were separated from CD4− lymphocytes using CD4+ T-Cell Isolation Kit (Miltenyi Biotec). The purity and Vβ usage of CD3+CD4+CD26− T-cells were confirmed by flow cytometry; all CD4+ T-cell samples had a purity of > 90%. The CD4− cells were also collected, from which DNAs were isolated and used as a second matched control for identification of somatic mutations. Our analysis suggested contamination of Sézary cells in the CD4− cell population (data not shown) and thus matched fibroblast DNAs were used as germline controls for somatic mutation and copy number analyses.

Skin punch biopsy and fibroblast cell culture

A 6-mm biopsy of normal skin from the inner arm was performed for all patients. Explanted fibroblasts were grown and maintained in Dulbecco's MEM supplemented with non-essential amino acids, 1% penicillin/streptomycin, 1% HEPES, 1% sodium pyruvate, and 10% fetal bovine serum (DMEM-FBS) at 37°C in humidified air containing 5% CO_2. Fibroblasts were subcultured using trypsin/EDTA. DNA and total RNA was extracted at passage 3 to 4[64].

DNA/RNA extraction

For all samples, about 5×10^6 cells were collected and genomic DNA and total RNA were extracted simultaneously using All Prep DNA/RNA/Protein Mini Kit (QIAGEN) following the manufacturer's protocol.

WES library preparation, exome capture and sequencing

DNA samples were constructed into Illumina paired-end (PE) pre-capture libraries as previously described[28] with minor modifications. Briefly, 0.5 μg DNA was sheared into fragments of 200–300 base pairs in a Covaris plate with E210 system (Covaris) followed by end-repair, A-tailing and ligation of Illumina multiplexing PE adaptors. Pre-capture Ligation Mediated-PCR (LM-PCR) was performed using the Library Amplification Readymix containing KAPA HiFi DNA Polymerase (Kapa Biosystems, Cat. No. KK2612). Universal primer IMUX-P1.0 and IMUX-P3.0 were used in PCR amplification. For a sub-set of the libraries constructed in this study, these molecular barcodes were introduced at PCR step using Phusion PCR Supermix HiFi (2X) (NEB, Cat. No. M0531L). Purification was performed with Agencourt AMPure XP beads after enzymatic reactions. Following the final XP beads purification, quantification and size distribution of the pre-capture LMPCR

product was determined using the LabChip GX electrophoresis system (PerkinElmer) and gel analysis using AlphaView SA v3.4 software.

For the hybridization step, four such pre-capture libraries were pooled together. The pooled libraries were then hybridized in solution to the HGSC VCRome 2.1 design. For post-capture LM-PCR amplification, either matching KAPA HiFi DNA Polymerase or Phusion PCR Supermix HiFi (2×) was used. After the final AMPure XP bead purification, quantity and size of the capture library was analyzed using the Caliper LabChip GX electrophoresis system. The efficiency of the capture was evaluated by performing a qPCR-based quality check on the enrichment level of four standard NimbleGen control loci. All sequencing runs were performed in PE mode on Illumina HiSeq2000 platform.

WES data processing, mutation calling and filtering

WES data processing, mutation calling and annotation was performed using the standard pipelines established at HGSC as described previously[28]. A stepwise filtering approach was performed to identify high-confident somatic mutations. Briefly, the quality filters we first applied and only those meeting the following criteria were selected: 1) the total read coverage in tumor and its matched control sample 5 and 2, respectively; 2) the variant read coverage in tumor 2; 3) the variant allele fraction (VAF) in tumor 0.04; 4) the ratio of VAF in normal and its tumor 0.15. Secondly, the germline filters were applied and any variants observed in the germline MAF file of the cohort were removed. After that, common SNPs were filtered out using dbSNP139 and virtual normals. Finally, all mutations left were visualized in Integrative Genomics Viewer (IGV, see URLs) and the mapping quality and uniqueness of the supporting reads was assessed using BLAT (see URLs). The ones with ambiguous mapping and poor mapping quality were removed from the list.

Mutation significance

The statistical significance of mutation frequency in each gene was determined using the MutSigCV algorithm (v1.4)[65] and our in-house BCMsig method. For MutSigCV analysis, a p value of < 0.05 and a q value (false discovery rate) of < 0.1 were considered statistically significant. Given that application of MutSigCV to our dataset revealed only two significantly mutated genes, we employed an alternative approach that is more sensitive to SMG identification for smaller tumor datasets. BCMsig is a simple binary algorithm that borrows elements from MutSigCV, but also incorporates other parameters, such as RNA expression data in both normal T-cells and SS cells, the cancer mutation literature, and likely functional impact of individual mutations. Analysis of the final somatic mutation file for 37 SS patients revealed 480 genes that had at least two non-silent somatic mutations. For each of these genes 13 parameters were analyzed and given scores of −1, 0, or +1, as indicated in rows 1-4 in **Supplementary Table 7**. Scores for each of the 13 parameters were added up and given a total score. All genes with a total score equal to or greater than that of *TP53* (9 points) were considered to be significantly mutated.

Mutation signatures

Non-negative matrix factorization (NMF) was used to evaluate the mutation signatures associated with SS malignant cells, of which there was a set of 21 available. Mutation data

were transformed into a data matrix $\mathbf{V}_{96,n}$ by normalizing and grouping mutations for each of the 16 mutation contexts (and 6 possibly base changes) for each of n subjects. Solutions were generated by solving the equation: $\mathbf{V} = \mathbf{W} \times \mathbf{H} + \mathbf{E}$ where $\mathbf{W}_{96,21}$ is the basis matrix of the NMF (Covington and Wheeler in preparation) solution and $\mathbf{H}_{21,n}$ is the coefficient matrix for the set of SS subjects, subject to minimizing the squared error ($\mathbf{E}$). $\mathbf{H}$ was taken as the set of overall signature exposure values, commonly referred to as the coefficient matrix. $\mathbf{H}$ can be taken to mean the number of mutations in a patient's sample attributable to each signature (see **Supplementary Fig. 4a and b**). $\mathbf{H}$ was also scaled such that each column of $\mathbf{H}$ summed to 1 to represent the proportion of mutations attributable to each signature (see **Figure 1b**). Both scaled and unscaled exposure values were merged with clinical, genomic, and transcritpomic data for further analysis.

Mutation validation and mutation prevalence

Thirty-five frequently altered genes were selected and a custom NimbleGen array (target size: ~200kb, **Supplementary Table 4**) was designed for mutation validation and mutation frequency screening. A total of 142 DNA samples were collected from patients in our combined cohorts. 0.1–0.5 µg DNA per sample was used for validation study.

The basic Illumina library preparation protocol and the regents used were identical to that of WES except that for validation, a set of 96 molecular barcodes were used to allow high density multiplexing. The capture enrichment protocol was also same as described earlier for WES, with the following modifications: for capture, four pools of 35–36 libraries/pool were prepared and hybridized in solution to the custom capture design. Overnight hybridization at 56°C was carried out instead of the 3-day hybridization at 47°C as done for WES. Post enrichment steps were also similar: four enriched pools were pooled into two groups (70 and 72 libraries/pool) and sequenced on two lanes of HiSeq 2500. On an average, 500 Mb of uniquely mapped sequence data were generated across the target region and the targeted bases were covered to 1226×.

For paired samples, the workflow of data processing was similar to that of WES. The mutation is valid if 5 or more supporting reads were detected. For tumor only samples, a stepwise filtering approach was applied to identify high-confident potential somatic mutations. Briefly, only non-silent mutations with 5 supporting reads and a VAF of 0.01 were selected, the common SNPs were eliminated using dbSNP database and virtual normals. The list was further cleaned by removing variants present in any of the fibroblast controls. Finally, all left mutations were visualized in IGV and the mapping quality and uniqueness of the supporting reads was assessed using BLAT. The ones with ambiguous mapping and poor mapping quality were removed from the list.

RNA-seq library construction, sequencing, and quality control

High quality total RNA (RIN > 7) was used to prepare strand-specific, poly-A$^+$ Illumina RNA-seq libraries. To monitor sample and process variability, in addition to sequence metrics, RNA developed by the External RNA Controls Consortium (ERCC) which consists of a mix of 92 polyadenylated RNA transcripts was also added to total RNA at the beginning of the library preparation. Briefly, poly-A$^+$ mRNA was extracted from 1 µg total RNA using

Oligo(dT)$_{25}$ Dynabeads (Life Technologies, Cat. No. 61002) followed by fragmentation, first strand cDNA synthesis, second strand cDNA synthesis, end-repair, A-tailing, ligated with Illumina PE adapters, and then digested with 10 units of Uracil-DNA Glycosylase (NEB, Cat. No. M0280L). Amplification of the libraries was performed for 13–14 PCR cycles using the Phusion High-Fidelity PCR Master Mix; twelve such 6-bp molecular barcodes were also incorporated during this PCR amplification. The cDNA was purified with Agencourt AMPure XP beads after each enzymatic reaction, and after quantification using the Agilent Bioanalyzer 2100 DNA Chip 7500 (Cat. No. 5067-1506). Libraries were pooled in equimolar amounts (2 – 5 libraries/pool). The library pools were then loaded onto a HiSeq flowcell lane, and following amplification with Illumina's cBot cluster generation system, sequencing runs were performed in PE mode (2×101 bp reads) using the Illumina HiSeq2000 and HiSeq 2500 platforms. The data generated was processed through an automated RNA-Seq pipeline built for quality control, gene fusion and expression analysis. RNA-SeQC (v1.1.7)[66] was applied to generate a series of quality control metrics for RNA-seq data.

Expression quantification and differential gene expression

The FASTQ data generated from production pipeline were mapped to human genome (both hg19 and known splice junction loci) using the STAR RNA-seq aligner (v2.3.1)[67]. The human genome and gene models (GRCh37.69) were downloaded from Ensembl (see URLs). The transcripts were then assembled with Cufflinks (v2.1.1)[68] and the expression level of each gene was calculated and normalized.

Gene fusion detection and filtering

To identify gene fusion transcripts, RNA-seq reads in FASTQ format were aligned to human genome by deFuse algorithm (v0.6.1)[69]. DeFuse was run with default parameters and a probability score was assigned to each candidate with DeFuse classifier. The candidate gene fusion transcripts were filtered step by step to identify the high-confident fusion events. Briefly, the fusion transcripts with preservation of the open reading frame and with a probability score of > 0.3 were selected. The mapping uniqueness of each fusion contig was assessed using BLAT and the ones with ambiguous mapping were removed. After that, the supporting reads for each fusion event were visualized in IGV and remapped using BLAT. Similarly, only those correctly mapped to the annotated positions were counted as supporting reads. Finally, fusion transcripts with 3 or more supporting reads were selected for validation.

Fusion gene validation

Validations of fusion transcripts were carried out via PCR amplification of first strand cDNA followed by Illumina MiSeq sequencing of the amplicon pools. Validation primers (shown in **Supplementary Table 11**) were designed using Primer 3 program (see URLs). For each validation event, one oligonucleotide matching each end of the splitter was picked as forward and reverse primer to generate amplicons containing the breakpoints of the fusion RNAs. Briefly, 200 ng total RNA was used to prepared first strand cDNA and the first strand cDNA was amplified on Eppendorf Mastercycler ep384 (Eppendorf, Westbury, NY) with

TaKaRa LA Taq DNA Polymerase, Hot-Start version (Cat no. RR042, Clontech). PCR products were examined and further purified. Amplicons with low yield were subjected to another round PCR program above with 2% of first round PCR products as template. Purified PCR products were equally pooled for Illumina library construction. 2 pools of 29 amplicons were sequenced on a Miseq sequencer.

Sequencing reads were aligned to human genome as described above for RNA-seq data. For each fusion event, its corresponding validation bam file was loaded to and visualized in IGV. The sequences of the supporting reads were extracted and remapped using BLAT to confirm the fusion breakpoints.

Mutation cross validation with RNA-seq data

RNA-seq data were also used to cross validate the somatic mutations identified by WES. For each somatic mutation reported by WES, SAMtools (v0.1.8)[70] was used to count the read coverage for the variant and reference alleles in corresponding RNA-seq BAM files. A minimum of one high-quality supporting read was required to define a validated mutation. The validation results were summarized into the following 4 different conditions: validated with VAF > 5%; validated with VAF <5%; mutant allele not expressed if the mutation site was covered well but no mutant allele was detected; no information if no reads were mapped to the particular mutation site or gene.

TCR clonality analysis

The Gencode Genes (v18, see URLs) was used for annotation of the TCR loci. The igvtools (see URLs) was used to extract the base coverage of the corresponding TCR loci from RNA-seq BAM files for all samples. Wiggle files were generated for each sample and loaded into IGV for further analysis. The read scale was adjusted between the tumor and control samples for a better visualization.

SNP array and DNA copy number

Infinium SNP array assays were performed with Illumina Human OmniExpress12 v1-1 BeadChips (Cat. no. WG-312-1120). In brief, 200 ng genomic DNA was denatured, followed by isothermal whole genome amplification. The amplified DNA was enzymatically fragmented and hybridized to BeadChip for 16–24 hours at 48°C in hybridization oven. Twelve samples were processed in parallel on each BeadChip. A series of washing steps were conducted to remove unhybridized and non-specifically hybridized DNA fragments from the BeadChips, followed by allele-specific single-base extension reaction and multi-layer staining process. The coated BeadChips were imaged using Illumina iScan system. The SNP calls were collected using the Illumina GenomeStudio v2011.1 software. Cutoff for SNP call rate was set at 0.9 and data from samples passing this metric were used for further analyses.

For improved CNV analysis, B allele frequencies (BAF) were calculated and $\log_2$ R ratios (LRR) were extracted after re-clustering the raw data by applying the GenomeStudio clustering algorithms. The BAF and LRR data were then loaded into Nexus Copy Number v7.5 (BioDiscovery) to identify somatic DNA copy number alterations in SS patients.

Systematic correction was applied to all samples with parameter settings refined for Illumina OmniExpress platform to correct the GC content related data waviness. The SNP-FASST2 segmentation algorithm was selected and matched paired analysis was performed following the manufacture's manual. Significant peaks were selected with a p-value cut-off of 0.05 and the aggregating frequency cut-off of 20%.

IL32 ELISA

The human CTCL cell lines HH, Hut78 and MJ were purchased from American Type Culture Collection (ATCC) (Manassas, VA). Other cell lines were kind gifts from Dr. Ivan Litvinov (Department of Medicine, McGill University, Canada). Cells were grown at 0.2–1.0×10^6/ml in HEPES-buffered RPMI 1640 medium as previously described[14]. Cell culture supernatants were collected on Day 3 after the media were refreshed. 8 ml of whole blood from patients were collected into a red-topped tube without additives, kept at RT for 30 minutes, and then centrifuged for 10 minutes at $1,000 \times g$. The serum layers were then removed and aliquoted into small tubes and store at $-80°C$ until use. The 5 normal human serum samples were purchased from different vendors and aliquot into small tubes and store at $-80°C$ until use.

Soluble IL-32α in cell culture supernatants and human sera were measured using the Human IL-32α ELISA MAX™ Deluxe Sets (Biolegend, San Diego, CA). Briefly, the day before the assay, 100 μL/well of 1:200 capture antibody coating solution was added and the plate was incubated overnight at 4°C. Washing was performed immediately after each of the following steps to removed non-specific antibody binding. 200 μl/well of 1X Assay Diluent A was added and the plate was incubated at room temperature (RT) for 1 hour to block non-specific binding. After that, 100 μL/well of standards or samples were added and the plate was incubated at RT for 2 hours. The human IL-32α standard concentrations used were 500 pg/mL, 250 pg/mL, 125 pg/mL, 62.5 pg/mL, 31.3 pg/mL, 15.6 pg/mL, and 7.8 pg/mL, respectively. 1X Assay Diluent A serves as the zero standard (0 pg/mL). All standards were run in duplicate, and all samples were run in triplicate. After washing, 100 μL/well of 1:200 diluted Detection Antibody solution was added and the plate was incubated at RT for 1 hour. 100 μL/well of 1:1000 diluted Avidin-HRP solution was added and the plate was incubated at RT for 30 minutes. The plates were then developed with 100 μL/well of freshly mixed TMB Substrate Solution in the dark for 10-15 minutes followed by adding 100 μL/well of Stop Solution. The plates were read at 450 nm within 30 minutes. Concentrations were calculated and the data were shown as the mean of triplicate determinations.

IL32 Western Blot

The extracted cellular proteins were fractionated and transferred onto nitrocellulose membranes by electro-blotting. After being blocked in 5% milk in TBS supplemented with 0.05% Tween 20 for 1 hour at RT, the membranes were incubated with purified mouse anti-human IL-32αβδγ antibody IgG1, κ (Clone KU32-52, 1:1,000, Biolegend, San Diego, CA) overnight at 4 °C in 5% milk in TBST. The membranes were washed with TBST and then incubated with 1:1,000 HRP-conjugated goat anti-mouse polyclonal secondary antibodies (Cell Signaling, Beverly, MA) for 1 hour at RT. After washing with TBS, antibody binding was visualized using enhanced chemiluminescence (the SuperSignal™ West Pico

Chemiluminescence Substrate, Thermo Fisher Scientific, Rockford, IL). The equivalent loading of proteins in each well was confirmed by Ponceau staining and actin control.

Supplementary Material

Refer to Web version on PubMed Central for supplementary material.

ACKNOWLEDGEMENTS

References

1. Campbell JJ, Clark RA, Watanabe R, Kupper TS. Sezary syndrome and mycosis fungoides arise from distinct T-cell subsets: a biologic rationale for their distinct clinical behaviors. Blood. 2010; 116:767–71. [PubMed: 20484084]

2. Girardi M, Heald PW, Wilson LD. The pathogenesis of mycosis fungoides. N Engl J Med. 2004; 350:1978–88. [PubMed: 15128898]

3. Kim YH, Liu HL, Mraz-Gernhard S, Varghese A, Hoppe RT. Long-term outcome of 525 patients with mycosis fungoides and Sezary syndrome: clinical prognostic factors and risk for disease progression. Arch Dermatol. 2003; 139:857–66. [PubMed: 12873880]

4. Olsen E, et al. Revisions to the staging and classification of mycosis fungoides and Sezary syndrome: a proposal of the International Society for Cutaneous Lymphomas (ISCL) and the cutaneous lymphoma task force of the European Organization of Research and Treatment of Cancer (EORTC). Blood. 2007; 110:1713–22. [PubMed: 17540844]

5. Jawed SI, Myskowski PL, Horwitz S, Moskowitz A, Querfeld C. Primary cutaneous T-cell lymphoma (mycosis fungoides and Sézary syndrome): part I. Diagnosis: clinical and histopathologic features and new molecular and biologic markers. Journal of the American Academy of Dermatology. 2014; 70:205, e1–16. quiz 221-222. [PubMed: 24438969]

6. Venkatarajan S, Duvic M. Sézary syndrome: an overview of current and future treatment options. Expert opinion on orphan drugs. 2014; 2:3.

7. Herne KL, Talpur R, Breuer-McHam J, Champlin R, Duvic M. Cytomegalovirus seropositivity is significantly associated with mycosis fungoides and Sezary syndrome. Blood. 2003; 101:2132–6. [PubMed: 12446446]

8. Talpur R, Bassett R, Duvic M. Prevalence and treatment of Staphylococcus aureus colonization in patients with mycosis fungoides and Sezary syndrome. Br J Dermatol. 2008; 159:105–12. [PubMed: 18489588]

9. Agar NS, et al. Survival outcomes and prognostic factors in mycosis fungoides/Sezary syndrome: validation of the revised International Society for Cutaneous Lymphomas/European Organisation for Research and Treatment of Cancer staging proposal. J Clin Oncol. 2010; 28:4730–9. [PubMed: 20855822]

10. Scarisbrick JJ, et al. Prognostic factors, prognostic indices and staging in mycosis fungoides and Sezary syndrome: where are we now? Br J Dermatol. 2014; 170:1226–36. [PubMed: 24641480]

11. Talpur R, et al. Long-term outcomes of 1,263 patients with mycosis fungoides and Sezary syndrome from 1982 to 2009. Clin Cancer Res. 2012; 18:5051–60. [PubMed: 22850569]

12. Vidulich KA, Talpur R, Bassett RL, Duvic M. Overall survival in erythrodermic cutaneous T-cell lymphoma: an analysis of prognostic factors in a cohort of patients with erythrodermic cutaneous T-cell lymphoma. Int J Dermatol. 2009; 48:243–52. [PubMed: 19261011]

13. Kim EJ, et al. Immunopathogenesis and therapy of cutaneous T cell lymphoma. J Clin Invest. 2005; 115:798–812. [PubMed: 15841167]

14. Ni X, Zhang C, Talpur R, Duvic M. Resistance to activation-induced cell death and bystander cytotoxicity via the Fas/Fas ligand pathway are implicated in the pathogenesis of cutaneous T cell lymphomas. J Invest Dermatol. 2005; 124:741–50. [PubMed: 15816832]

15. Batista DA, et al. Multicolor fluorescence in situ hybridization (SKY) in mycosis fungoides and Sezary syndrome: search for recurrent chromosome abnormalities. Genes Chromosomes Cancer. 2006; 45:383–91. [PubMed: 16382449]

16. Caprini E, et al. Identification of key regions and genes important in the pathogenesis of sezary syndrome by combining genomic and expression microarrays. Cancer Research. 2009; 69:8438–8446. [PubMed: 19843862]

17. Mao X, Chaplin T, Young BD. Integrated genomic analysis of sézary syndrome. Genetics Research International. 2011; 2011:980150. [PubMed: 22567373]

18. Mao X, et al. Molecular cytogenetic characterization of Sezary syndrome. Genes Chromosomes Cancer. 2003; 36:250–60. [PubMed: 12557225]

19. Vermeer MH, et al. Novel and highly recurrent chromosomal alterations in Sézary syndrome. Cancer Research. 2008; 68:2689–2698. [PubMed: 18413736]

20. Braun FCM, et al. Tumor suppressor TNFAIP3 (A20) is frequently deleted in Sezary syndrome. Leukemia. 2011; 25:1494–1501. [PubMed: 21625233]

21. Laharanne E, et al. CDKN2A-CDKN2B deletion defines an aggressive subset of cutaneous T-cell lymphoma. Mod Pathol. 2010; 23:547–58. [PubMed: 20118908]

22. Lamprecht B, et al. The tumour suppressor p53 is frequently nonfunctional in Sézary syndrome. The British Journal of Dermatology. 2012; 167:240–246. [PubMed: 22384858]

23. Vaqué JP, et al. PLCG1 mutations in cutaneous T-cell lymphomas. Blood. 2014; 123:2034–2043. [PubMed: 24497536]

24. Ungewickell A, et al. Genomic analysis of mycosis fungoides and Sezary syndrome identifies recurrent alterations in TNFR2. Nat Genet. 2015; 47:1056–60. [PubMed: 26258847]

25. Choi J, et al. Genomic landscape of cutaneous T cell lymphoma. Nat Genet. 2015; 47:1011–9. [PubMed: 26192916]

26. Duvic M, Foss FM. Mycosis fungoides: pathophysiology and emerging therapies. Semin Oncol. 2007; 34:S21–8. [PubMed: 18086343]

27. Horwitz SM. Novel therapies for cutaneous T-cell lymphomas. Clin Lymphoma Myeloma. 2008; 8(Suppl 5):S187–92. [PubMed: 19073526]

28. Wang L, et al. Novel somatic and germline mutations in intracranial germ cell tumours. Nature. 2014; 511:241–5. [PubMed: 24896186]

29. Lawrence MS, et al. Discovery and saturation analysis of cancer genes across 21 tumour types. Nature. 2014; 505:495–501. [PubMed: 24390350]

30. Wheeler DA, Wang L. From human genome to cancer genome: the first decade. Genome Res. 2013; 23:1054–62. [PubMed: 23817046]

31. Alexandrov LB, et al. Signatures of mutational processes in human cancer. Nature. 2013; 500:415–21. [PubMed: 23945592]

32. Clark RA. Resident memory T cells in human health and disease. Sci Transl Med. 2015; 7:269rv1.

33. Wu XS, Lonsdorf AS, Hwang ST. Cutaneous T-cell lymphoma: roles for chemokines and chemokine receptors. J Invest Dermatol. 2009; 129:1115–9. [PubMed: 19242508]

34. Yoshie O, Matsushima K. CCR4 and its ligands: from bench to bedside. Int Immunol. 2015; 27:11–20. [PubMed: 25087232]

35. Ni X, et al. Reduction of regulatory T cells by Mogamulizumab, a defucosylated anti-CC chemokine receptor 4 antibody, in patients with aggressive/refractory mycosis fungoides and Sezary syndrome. Clin Cancer Res. 2015; 21:274–85. [PubMed: 25376389]

36. Duvic M, et al. Phase 1/2 study of mogamulizumab, a defucosylated anti-CCR4 antibody, in previously treated patients with cutaneous T-cell lymphoma. Blood. 2015

37. Nakagawa M, et al. Gain-of-function CCR4 mutations in adult T cell leukemia/lymphoma. J Exp Med. 2014; 211:2497–2505. [PubMed: 25488980]

38. Matsumoto R, et al. Phosphorylation of CARMA1 plays a critical role in T Cell receptor-mediated NF-kappaB activation. Immunity. 2005; 23:575–585. [PubMed: 16356856]

39. Hara H, et al. The MAGUK family protein CARD11 is essential for lymphocyte activation. Immunity. 2003; 18:763–75. [PubMed: 12818158]

40. Wang D, et al. A requirement for CARMA1 in TCR-induced NF-kappa B activation. Nature Immunology. 2002; 3:830–835. [PubMed: 12154356]

41. Lohr JG, et al. Discovery and prioritization of somatic mutations in diffuse large B-cell lymphoma (DLBCL) by whole-exome sequencing. Proceedings of the National Academy of Sciences of the United States of America. 2012; 109:3879–3884. [PubMed: 22343534]

42. Lenz G, et al. Oncogenic CARD11 mutations in human diffuse large B cell lymphoma. Science (New York, N.Y.). 2008; 319:1676–1679.

43. Dereure O, Portales P, Clot J, Guilhou JJ. Decreased expression of Fas (APO-1/CD95) on peripheral blood CD4+ T lymphocytes in cutaneous T-cell lymphomas. Br J Dermatol. 2000; 143:1205–10. [PubMed: 11122022]

44. Jones CL, et al. Downregulation of Fas gene expression in Sézary syndrome is associated with promoter hypermethylation. The Journal of Investigative Dermatology. 2010; 130:1116–1125. [PubMed: 19759548]

45. Postigo AA, Dean DC. Independent repressor domains in ZEB regulate muscle and T-cell differentiation. Mol Cell Biol. 1999; 19:7961–71. [PubMed: 10567522]

46. Higashi Y, et al. Impairment of T cell development in deltaEF1 mutant mice. J Exp Med. 1997; 185:1467–79. [PubMed: 9126927]

47. Nakahata S, Yamazaki S, Nakauchi H, Morishita K. Downregulation of ZEB1 and overexpression of Smad7 contribute to resistance to TGF-beta1-mediated growth suppression in adult T-cell leukemia/lymphoma. Oncogene. 2010; 29:4157–69. [PubMed: 20514018]

48. Hidaka T, et al. Down-regulation of TCF8 is involved in the leukemogenesis of adult T-cell leukemia/lymphoma. Blood. 2008; 112:383–93. [PubMed: 18467597]

49. Blais A, Dynlacht BD. E2F-associated chromatin modifiers and cell cycle control. Curr Opin Cell Biol. 2007; 19:658–62. [PubMed: 18023996]

50. Nagl NG Jr. Wang X, Patsialou A, Van Scoy M, Moran E. Distinct mammalian SWI/SNF chromatin remodeling complexes with opposing roles in cell-cycle control. EMBO J. 2007; 26:752–63. [PubMed: 17255939]

51. Nam HJ, et al. The ERK-RSK1 activation by growth factors at G2 phase delays cell cycle progression and reduces mitotic aberrations. Cell Signal. 2008; 20:1349–58. [PubMed: 18450423]

52. Freeman GJ, et al. Engagement of the PD-1 immunoinhibitory receptor by a novel B7 family member leads to negative regulation of lymphocyte activation. J Exp Med. 2000; 192:1027–34. [PubMed: 11015443]

53. Okazaki T, Chikuma S, Iwai Y, Fagarasan S, Honjo T. A rheostat for immune responses: the unique properties of PD-1 and their advantages for clinical application. Nat Immunol. 2013; 14:1212–8. [PubMed: 24240160]

54. Suga H, et al. The role of IL-32 in cutaneous T-cell lymphoma. The Journal of Investigative Dermatology. 2014; 134:1428–1435. [PubMed: 24226419]

55. Ohmatsu H, et al. IL32 Is Progressively Expressed in Mycosis Fungoides Independent of Helper T-cell 2 and Helper T-cell 9 Polarization. Cancer Immunology Research. 2014; 2:890–900. [PubMed: 24938282]

56. Kim KH, et al. Interleukin-32 monoclonal antibodies for immunohistochemistry, Western blotting, and ELISA. J Immunol Methods. 2008; 333:38–50. [PubMed: 18252253]

57. Huether R, et al. The landscape of somatic mutations in epigenetic regulators across 1,000 paediatric cancer genomes. Nat Commun. 2014; 5:3630. [PubMed: 24710217]

58. Vega F, et al. Clonal heterogeneity in mycosis fungoides and its relationship to clinical course. Blood. 2002; 100:3369–73. [PubMed: 12384439]

59. Jackow CM, et al. Association of erythrodermic cutaneous T-cell lymphoma, superantigen-positive Staphylococcus aureus, and oligoclonal T-cell receptor V beta gene expansion. Blood. 1997; 89:32–40. [PubMed: 8978274]

60. Tan RS, Butterworth CM, McLaughlin H, Malka S, Samman PD. Mycosis fungoides--a disease of antigen persistence. Br J Dermatol. 1974; 91:607–16. [PubMed: 4281316]

61. Spits H. Development of alphabeta T cells in the human thymus. Nat Rev Immunol. 2002; 2:760–72. [PubMed: 12360214]

62. Murphy, KP.; Mowat, A.; Weaver, CT. Janeway's Immunobiology. Garland Science; 2011.

63. Bradford PT, Devesa SS, Anderson WF, Toro JR. Cutaneous lymphoma incidence patterns in the United States: a population-based study of 3884 cases. Blood. 2009; 113:5064–73. [PubMed: 19279331]

64. Takashima, A. Establishment of Fibroblast Cultures. in Current Protocols in Cell Biology. John Wiley & Sons, Inc.; 2001.

65. Lawrence MS, et al. Mutational heterogeneity in cancer and the search for new cancer-associated genes. Nature. 2013; 499:214–8. [PubMed: 23770567]

66. DeLuca DS, et al. RNA-SeQC: RNA-seq metrics for quality control and process optimization. Bioinformatics. 2012; 28:1530–2. [PubMed: 22539670]

67. Dobin A, et al. STAR: ultrafast universal RNA-seq aligner. Bioinformatics. 2013; 29:15–21. [PubMed: 23104886]

68. Roberts A, Pimentel H, Trapnell C, Pachter L. Identification of novel transcripts in annotated genomes using RNA-Seq. Bioinformatics. 2011; 27:2325–9. [PubMed: 21697122]

69. McPherson A, et al. deFuse: an algorithm for gene fusion discovery in tumor RNA-Seq data. PLoS Comput Biol. 2011; 7:e1001138. [PubMed: 21625565]

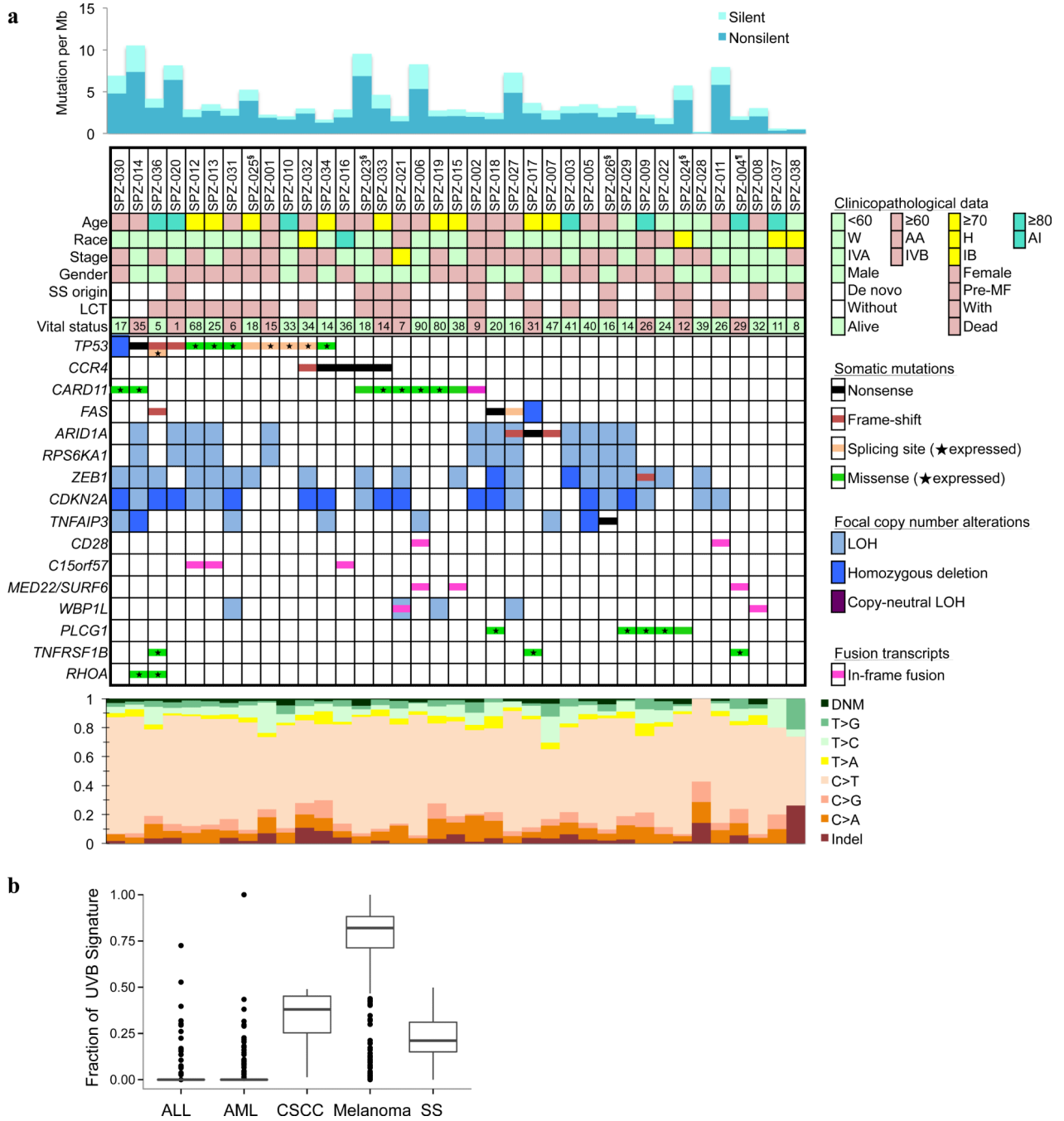70. Li H, et al. The Sequence Alignment/Map format and SAMtools. Bioinformatics. 2009; 25:2078–9. [PubMed: 19505943]

Fig. 1. Somatic genomic alterations identified in SS patients

a) The upper panel shows somatic mutation rates estimated by WES. The middle panel shows somatic mutations by patient (columns) and by gene (rows) including point mutations, somatic copy number alterations, and recurrent fusion transcripts. The top rows are patient IDs, followed by clinical and histopathological data. Race: W, White; AA, African American; H, Hispanic; AI, American Indian. SS origin: Pre-MF, pre-existing MF. LCT, large cell transformation. LOH, loss of heterozygosity. The number of months lived after disease diagnosis to last clinical visit or death was indicated together with the vital

status. Annotation of RNA-seq expression was added for all missense and splicing mutations. A star indicates that the mutant allele was observed in the corresponding transcripts from RNA-seq data. Only genes that met one of the following criteria were included in the table: significantly mutated genes (MutSigCV, false discovery rate <0.1; BCMsig, total points 9); significant focal copy number alterations; with in-frame fusions in 2 patients; cancer related or biologically important (overlap with Cancer Gene Census or MSigDB database, see URLs) and with 2 or more nonsense, frame-shift, or expressed missense mutations, and were replicated in the extension cohort. Bottom panel: the mutational spectral. DNM, dinucleotide mutations; Indel, small insertions and deletions. §RNA-seq was not performed; ¶SNP array was not performed, due to lack of materials. **b**) Prevalence of UVB signatures in SS and other cancer types.
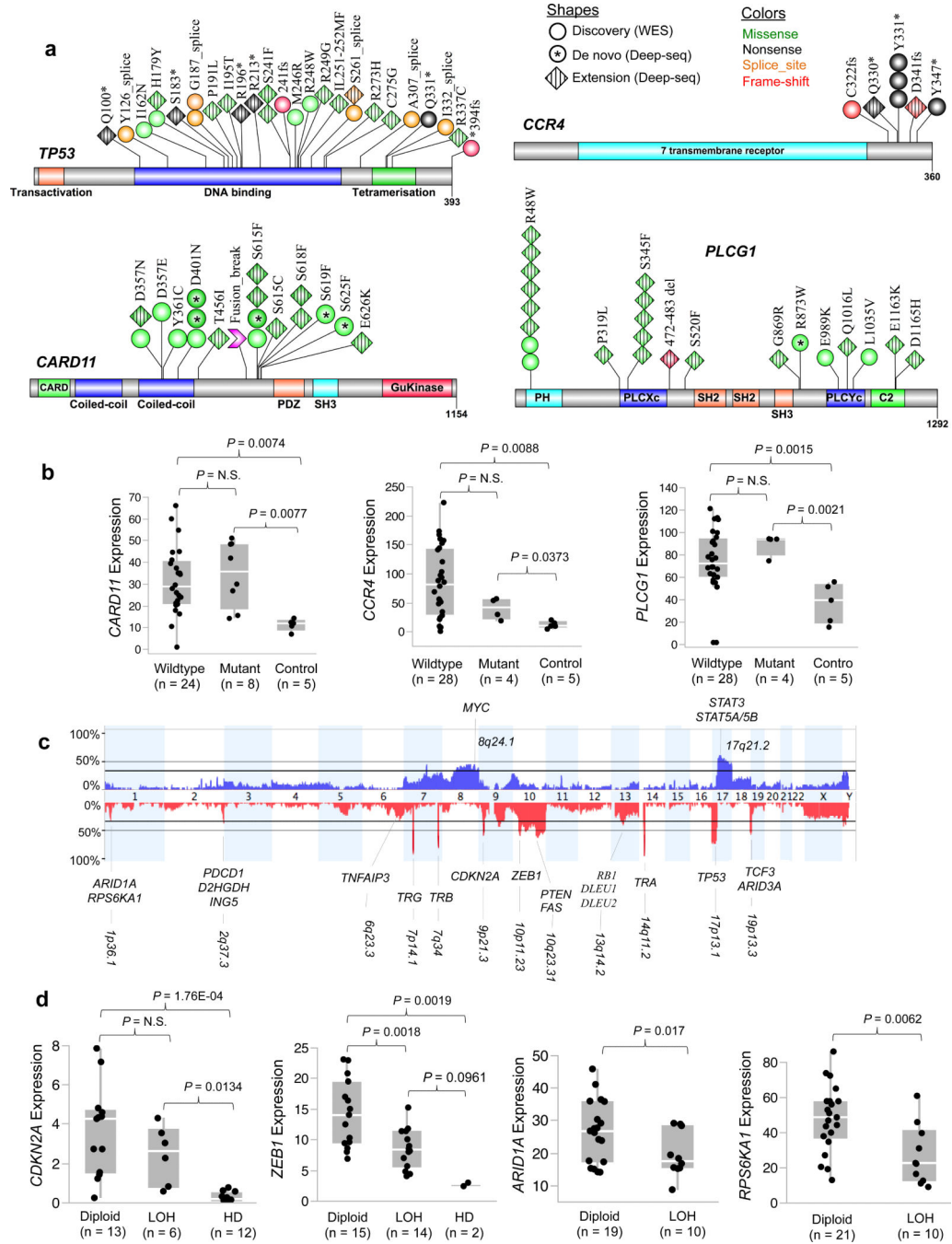
Fig. 2. Significant somatic mutation and copy number alterations

a) Schematic representation of somatic mutations identified in *TP53, CARD11, CCR4,* and *PLCG1*. The red arrowhead indicates the breakpoint for *CARD11* fusion; the coiled-coil domains of N-terminal portion are maintained in the fusion. **b**) Correlation analysis of somatic mutation and gene expression. Those five patients without RNA-seq data were excluded from the analysis. **c**) Aggregation of somatic copy number alterations. For all frequently occurred focal copy number alterations, the cytogenetic positions were indicated and the names of involved genes that have potential pathogenic significance were displayed;

bolded type face were for focal events. For chromosomal arm-level alterations, only the positions and names of well-known cancer-related genes were displayed. **d**) Correlation analysis of somatic copy number alteration and gene expression. The copy number status was inferred by Nexus (BioDiscovery, Inc.) analysis of the SNP array data. The gene expression levels were normalized FPKM values calculated by the Cufflinks algorithm using RNA-seq data. Those six patients without RNA-seq or SNP array data were excluded from the analysis. For *ARID1A* correlation analysis, two additional patients with inactivating *ARID1A* mutations were also excluded. P-values were calculated by one-way ANOVA and student t-test. LOH, loss of heterozygosity; HD, homozygous deletion.
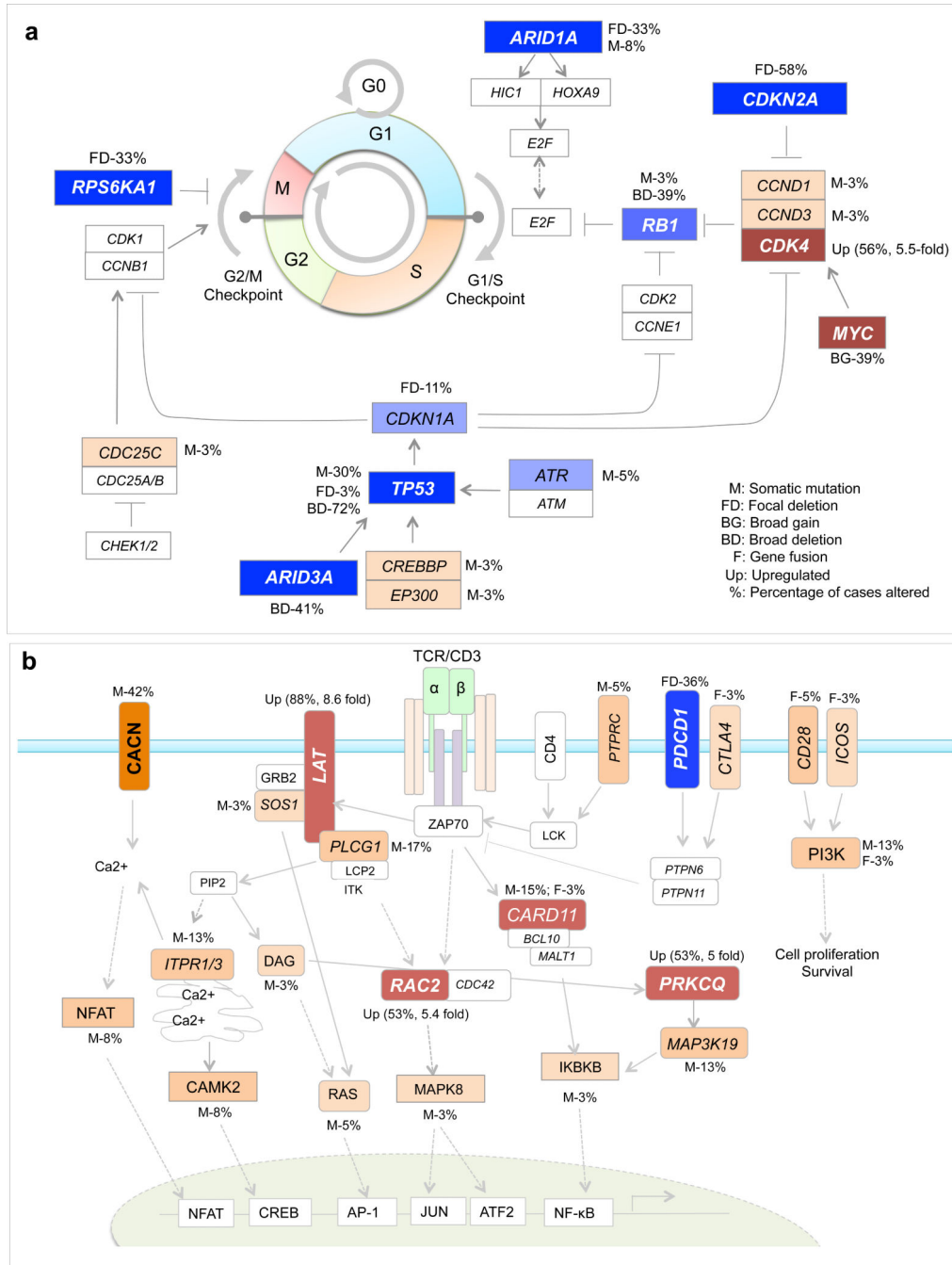
Fig. 3. The dysregulated signaling pathways

a) The cell cycle checkpoint machinery. **b)** T-cell receptor (TCR) signaling pathway. The genes with inactivating mutations or copy number losses were colored in blue; the genes with activating mutations, copy number gains or significantly upregulated genes in comparison with control T cells were colored in red; genes with all other genetic alterations were colored in orange; genes without detectable alterations but are important components of the pathway are also included and shown in white rectangles; for each gene with somatic

alterations, the percentage of cases altered was indicated; for significantly upregulated genes, the average fold changes are also shown.
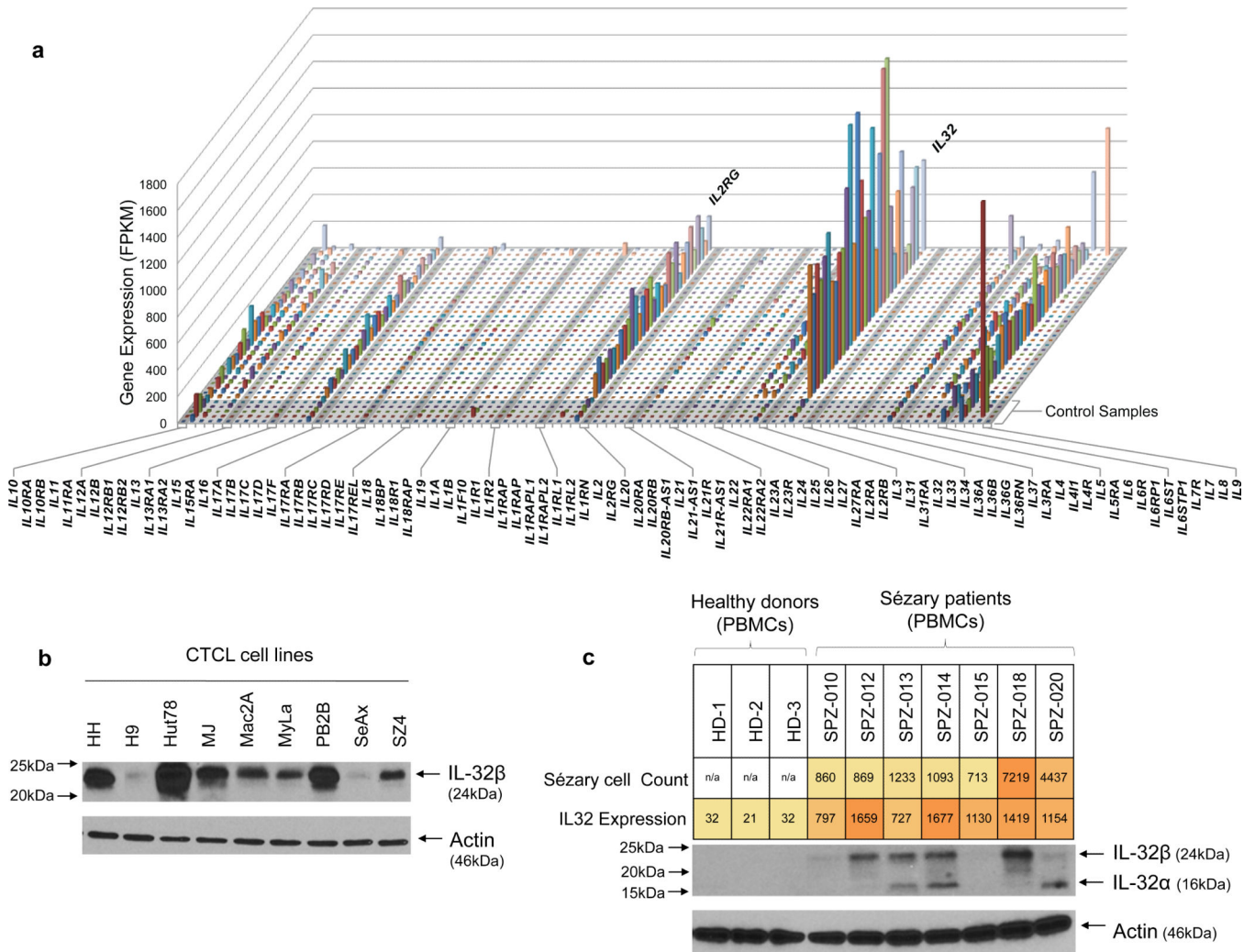
Fig. 4. Increased IL32 gene and protein expression
a) Expression profiles of all the interleukins in SS patients. The gene expression data were generated from RNA-seq. The five control samples were obtained from sorted CD4^{+} T cells from healthy donors. (**b**) The cellular IL32 protein expression in 9 CTCL cell lines. (**c**) IL32 protein expression in the peripheral blood mononuclear cells (PBMCs) from 3 healthy donors (HD-1, 2, 3) and 7 SS patients. The protein expression was assessed by western blot with anti-human IL32 monoclonal antibody. The overall IL32 gene expression levels estimated from RNA-seq data (on purified SS cells) and the number of circulating SS cells in patients' PBMCs were shown and color scaled.
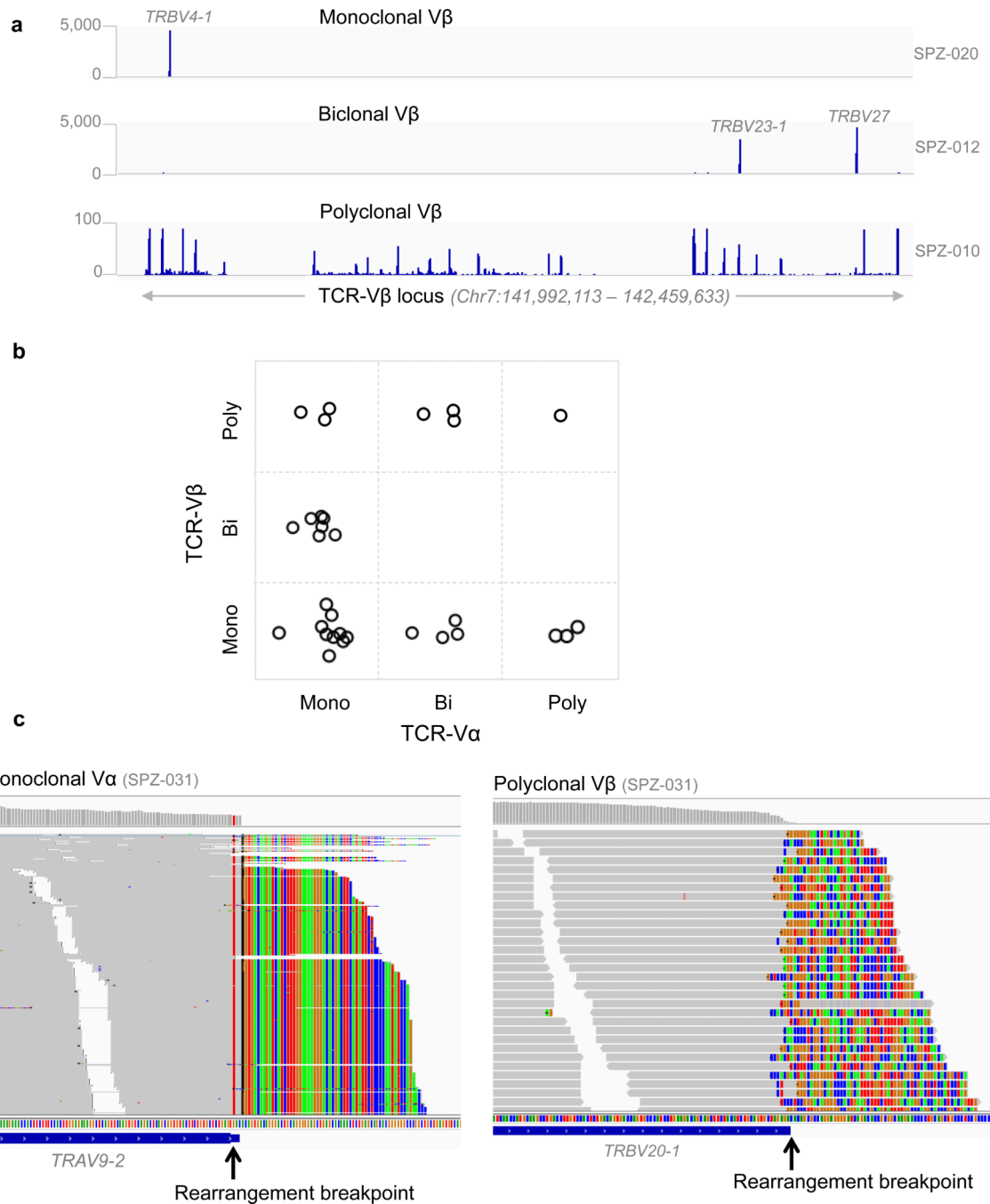
Fig. 5. Characterization of TCR clonality using RNA-seq

(**a**) Representative RNA-seq read coverage data showing the monoclonal, biclonal and polyclonal TCR-Vβ. The data ranges are shown on the left and the sample IDs are shown on the right. Clonally expressed TCR genes were indicated. **b**) The relationship of TCR-Vβ and Vα. Bi, biclonal; Mono, monoclonal; poly, polyclonal. Each circle represents a patient, which is placed in a box to indicate the state of its Vα and Vβ expression. **c**) Representative images showing partially aligned sequencing reads at the breakpoints of a TCR V-region rearrangement for a patient with monoclonal Vα and polyclonal Vβ. The matched

sequencing bases are in gray and the non-aligned bases shown color-coded (A, T, C, G; green, red, blue, brown, respectively) indicating the recombination break point where the V region adjoins its partner J region (Vα) or D region (Vβ). At the Vα exon all non-aligned reads exhibit the same sequence (note vertical striping of colors) indicating clonality in expression; at Vβ all non-aligned reads are different (note checkered pattern of colors) indicating polyclonal rearrangements of this V region.
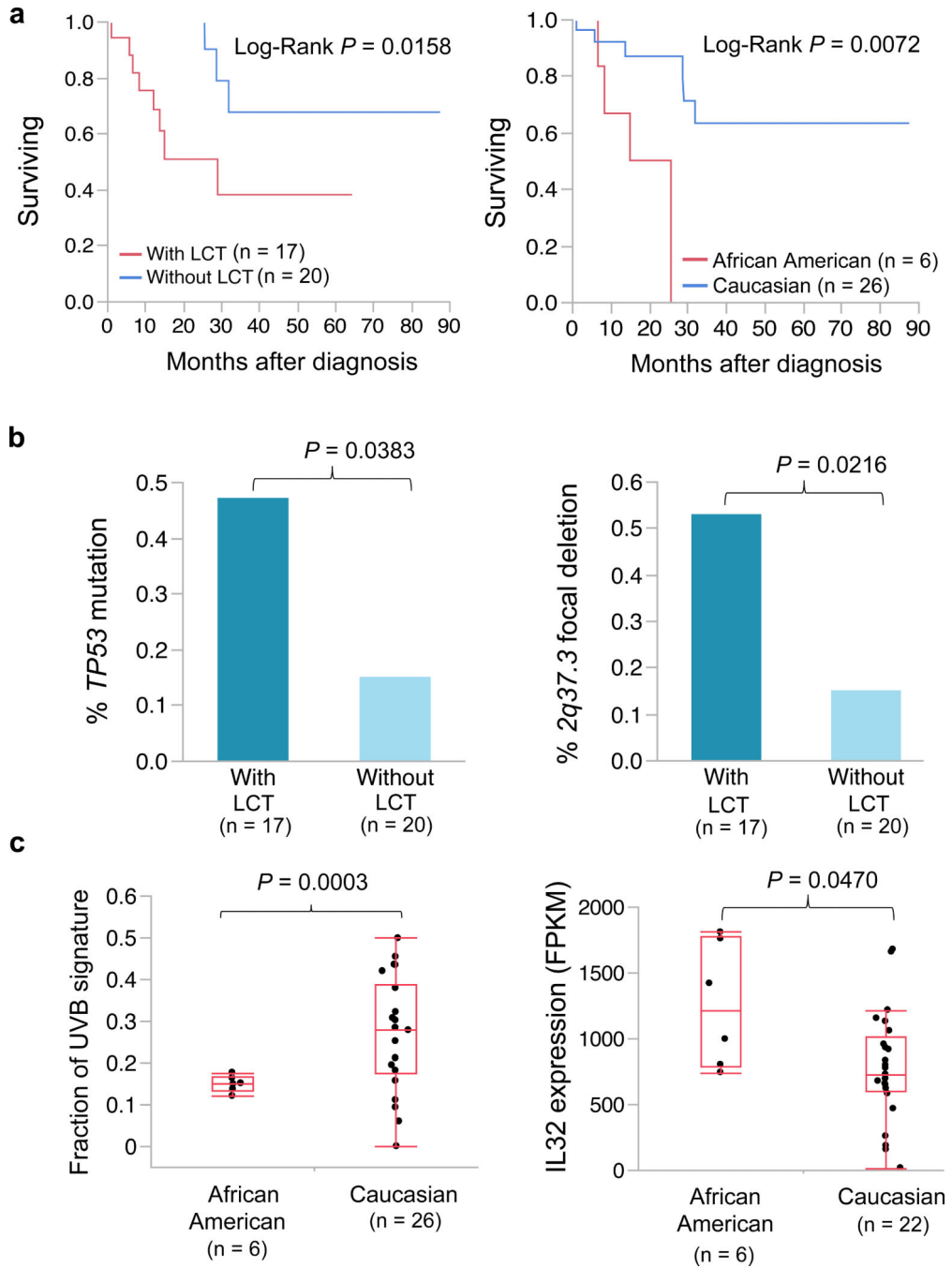
Fig. 6. Survival and correlation analysis

For survival analysis (**a**), the Kaplan-Meier survival plots were shown and the p-values were calculated by Log-Rank test. For frequency comparison (**b**), the p values were calculated by Fisher's exact test. For comparison of UVB signature and *IL32* expression, the p-values were calculated by t-test. Those four Caucasian patients without RNA-seq data were excluded from analysis.

Table 1

Significantly upregulated genes in SS patients that are important for T-cell function, pathogenesis or lineage significance

Gene	Gene_ID	Expression in tumor	Expression in control	Fold change	p value	q value	Gene function
IL2RG	ENSG00000147168	250.79	41.81	6.0	4.90E-15	1.98E-10	IL2, 4, 7 receptor activity, T-cell differentiation
IL32	ENSG00000008517	869.92	31.76	27.4	7.59E-12	3.07E-07	T-cell communication, proliferation
RAC2	ENSG00000128340	269.14	50.12	5.4	2.49E-11	1.01E-06	TCR signaling
LAT	ENSG00000213658	158.18	18.40	8.6	3.93E-11	1.59E-06	TCR signaling
GIMAP4	ENSG00000133574	206.62	7.29	28.3	5.19E-11	2.10E-06	Lymphocyte apoptosis, Th1/Th2 differentiation
IKZF2	ENSG00000030419	56.65	2.69	21.1	6.81E-11	2.75E-06	T-reg lymphocyte development
CD3G	ENSG00000160654	117.53	16.90	7.0	4.08E-10	1.65E-05	TCR signaling
TNFAIP8L2	ENSG00000163154	13.38	0.61	22.1	6.35E-10	2.57E-05	TCR function
SIT1	ENSG00000137078	44.85	7.03	6.4	1.07E-09	4.32E-05	TCR signaling
CD27	ENSG00000139193	114.42	7.18	15.9	1.49E-08	6.02E-04	T-cell differentiation, survival
PRKCQ	ENSG00000065675	32.50	6.45	5.0	3.43E-08	1.39E-03	TCR signaling
CCR4	ENSG00000183813	79.39	11.32	7.0	3.56E-07	1.44E-02	T-cell migration into skin
CCR8	ENSG00000179934	22.85	0.68	33.6	8.15E-07	3.30E-02	T-reg lymphocyte survival
IKBKE	ENSG00000143466	19.06	2.57	7.4	1.57E-12	6.36E-08	Oncogene: NF-κB and STAT signaling
CDK4	ENSG00000135446	17.64	3.18	5.5	1.13E-11	4.56E-07	Oncogene: cell cycle control
IL6R	ENSG00000160712	63.66	7.95	8.0	4.94E-10	2.00E-05	IL6 receptor activity, immune response
HRAS	ENSG00000174775	13.27	2.59	5.1	5.59E-10	2.26E-05	Oncogene
SLAMF6	ENSG00000162739	63.68	2.41	26.4	7.56E-09	3.05E-04	NK cell activation
TNFSF10	ENSG00000121858	85.09	7.43	11.40	4.00E-08	1.61E-03	Tumor necrosis factor, apoptosis
KLF8	ENSG00000102349	11.02	0.41	26.8	1.15E-07	4.63E-03	Cell cycle regulation, EMT
MYC	ENSG00000136997	41.45	8.13	5.1	3.83E-07	1.55E-02	Oncogene: cell cycle, apoptosis

TCR, T-cell receptor